Magnetic anisotropies and cationic distribution in CoFe2O4 nanoparticles prepared by co-precipitation route: Influence of particle size and stoichiometry

Niéli Daffé, Fadi Choueikani, Sophie Neveu, Marie-Anne Arrio, Amélie Juhin, Philippe Ohresser, Vincent Dupuis, Philippe Sainctavit

Magnetic anisotropies and cationic distribution in $CoFe_2O_4$ nanoparticles prepared by co-precipitation route: Influence of particle size and stoichiometry

Niéli Daffé[a, b, c, 1], Fadi Choueikani[c], Sophie Neveu[b], Marie-Anne Arrio[a], Amélie Juhin[a], Philippe Ohresser[c], Vincent Dupuis[b], Philippe Sainctavit[a, c, *]

[a] Institut de Minéralogie, de Physique des Matériaux et de Cosmochimie (IMPMC), UMR7590 CNRS, Université Pierre et Marie Curie, IRD, 4 Place Jussieu, 75052 Paris Cedex 05, France
[b] Sorbonne Université UPMC Univ Paris 06, UMR 8234, PHENIX, F-75005 Paris, France
[c] Synchrotron SOLEIL, L'Orme des Merisiers, Saint-Aubin – BP48, 91192 Gif-sur-Yvette, France

Keywords:
Nanoparticle
Magnetic anisotropies
XMCD
Spinels

A B S T R A C T

Magnetic anisotropies and crystallographic structures of cobalt-iron nanospinels obtained with the co-precipitation synthesis process are revealed using X-ray Absorption Spectroscopy and X-ray Magnetic Circular Dichroism. The chemical process allows to obtain nanoparticles of various sizes and chemical composition, but it is the site symmetry environment of Co^{2+} that is found to be the crucial parameter that governs the magnetic anisotropies of the nanospinels. The distribution of Co^{2+} among the crystallographic sites of the structure is directly linked to the temperature of the synthesis process. In parallel, the results also revealed that a superficial rich shell of iron is formed for the iron-cobalt nanospinels stable in acidic medium leading to chemically inhomogeneous nanoparticles.

1. Introduction

Ferro-/ferrimagnetic materials present attractive properties for modern applications due to the magnetic anisotropies arising from the system. Even more enhanced magnetic properties, not shown in the bulk, appear in the nanoscale of ferro-/ferrimagnetic materials. Such enhanced magnetic properties associated to the nanoscale range make them good candidates for applications in the biomedical field or for magnetic devices [1]. Approaches to use magnetic nanoparticles in biomedical applications rely on the large magnetization at saturation and on the large remanent magnetization of ferromagnetic materials that are mandatory for Magnetic Resonnance Imaging (MRI) [2] while advances in anticancer treatment take the advantage on the specific loss power of magnetic nanoparticles at radiofrequencies [3]. In the field of magneto-optical devices, integrated optics [4], core optical fibers [5] or tunable beam splitter [6] incorporate magnetic nanoparticles for their tunable magneto-optical properties. For such applications, ferrites with a spinel structure MFe_2O_4 (with M = Fe, Co, Mn, Ni, Zn…) present appealing properties [7]. Among them cobalt ferrite ($CoFe_2O_4$) is a promising magnetic material for high-storage devices [8] taking advantage of its large magneto-cristalline anisotropy energy [9], associated with a large coercive field H_c, and a moderate magnetization at saturation M_s. However the magnetic properties of $CoFe_2O_4$ nanoparticles can be strongly influenced by the morphology, the size, the chemical composition and the crystallographic structure. Ultimately, processes used to synthesize nanoparticles can be adjusted to the requirement of the application. In particular, chemical processes offer to tune a quasi-infinite number of parameters (chemical agents, pH, temperature, atmosphere and so on). During the last decades, various preparation modes of magnetic nanoparticles in fluids have been adopted [10–14]. Among them, the co-precipitation route [15] developed by R. Massart is a highly reliable, very convenient and cost-effective process to obtain well-crystallized and long term stable spinel nanoparticles dispersed in aqueous media. It is already known that the acidity of the medium or

Abbreviations: XMCD, O_h, T_d.

* Corresponding author at: Institut de Minéralogie, de Physique des Matériaux et de Cosmochimie (IMPMC), UMR7590 CNRS, Université Pierre et Marie Curie, IRD, 4 Place Jussieu, 75052 Paris Cedex 05, France.
Email address: Philippe.Sainctavit@upmc.fr (P. Sainctavit)
[1] Current address: Paul Scherrer Institut, PSI, 5232 Villigen, Switzerland.

the process temperature can influence the crystallographic order, the size, the shape and the stoichiometry of the nanocrystals, as well as the valence states of the cations [16,17].However, so far we know, it does not exist any systematic study linking the synthesis conditions of co-precipitation to the different magnetic properties of the nanospinels obtained. To obtain a clear picture of the relations existing between the co-precipitation synthesis conditions of iron-cobalt nanospinels and their magnetic properties, we have investigated six different sets of iron-cobalt nanospinels with different size and stoichiometry. The present study focuses on $Co_xFe_yO_4$ nanoparticles with sizes ranging from 7 to 21 nm and with molar ratios X_M equal to either 25% or to 33%. The cobalt molar ratio X_M is defined as follow:

$$X_M = \frac{[Co]}{[Co] + [Fe]} \quad (1)$$

$Co_xFe_yO_4$ crystallizes in the AB_2O_4 spinel structure that belongs to the $Fd\bar{3}m$ space group [18]. It is a face centered cubic (*fcc*) structure in which the oxygen anions O^{2-} are ordered in a cubic close-packed lattice. The rhombohedral unit cell contains two AB_2O_4 formula units, where A are tetrahedral sites (T_d) and B are octahedral ones (O_h). In direct spinels, T_d A sites are occupied by divalent ions whereas O_h B sites are occupied by trivalent ions. In inverse spinels, A sites are occupied exclusively by trivalent ions and B sites are occupied by both trivalent and divalent ions. Intermediate situations between direct and inverse spinels are characterized by a degree of inversion γ which is the fraction of divalent cations in octahedral sites. Hence, the cationic order of iron-cobalt spinels is described by Eq. (2) as:

$$[Co_{1-\gamma}Fe_{\gamma}]_{T_d}[Co_{\gamma}Fe_{2-\gamma}]_{O_h}O_4 \quad (2)$$

The inversion degree illustrates the crystallographic disorder. In the case of cubic spinels structure, the crystallographic order is deeply related to the magnetic anisotropies arising from the system. The crystallographic order of the nanoparticles have been investigated in various studies where the different cations distribution among T_d and O_h sites can be associated to different synthetic processes. Depending on the preparation mode of $CoFe_2O_4$ nanoparticles, inversion parameters from 0.20 to 0.96 have been obtained [19–23]. In parallel, Peddis and co-workers also established the major role played by surface spin-canting in the magnetic properties of small nanoparticles [19,24]. Among the technics used to characterized the cationic distributions in the spinels structure, if Mssbauer provides good results, more recently the composition and structure of Co-doped maghemite γ-Fe_2O_3 nanoparticles have been studied by Extended X-ray Absorption Fine Structure at the Fe and Co *K*-edge [25] and X-ray Absorption Near-Edges Spectra was used to study nanoparticles with different sizes prepared in a polyol medium [26]. In the present study, we investigate iron-cobalt nanospinels with X-ray Absorption Spectroscopy (XAS) and X-ray Magnetic Circular Dichroism (XMCD). These element selective spectroscopies have already been applied to investigate magnetic and cationic structure of such system [27–44]. As local probes of the electronic and magnetic properties, XAS and XMCD measurements allow to solve the crystallographic structure and disentangle the magnetic signature of Co^{2+} and Fe^{3+} in $CoFe_2O_4$ nanoparticles. In the following, we first describe the various coprecipitation synthesis routes that allowed to obtain the nanoparticles with variable sizes and X_M ratios, and then the characterization methods are detailed. Magnetometry measurements and XAS and XMCD results are presented and show that the magnetic properties of the nanospinels are not simply given by their composition and their size but are also governed by the organization on the cationic sublattices.

2. Experimental methods

2.1. Synthesis

The Co-precipitation synthesis yields nano-clusters dispersed in aqueous media with sizes ranging between 5 and 25 nm and different stoichiometries. We investigate here synthesis routes benefiting from significant improvements and new added treatments. In the following, the samples are named CoFeX_Y where X is the value of the molar ratio X_M and Y is the diameter in nm of the iron cobalt nanospinels. The list of the six nanospinels under study is reported in Table 1.

2.1.1. Co-precipitation route

The synthesis described in this paragraph leads to nanoparticles with a mean size of 9 nm and a molar ratio $X_M = 25\%$, named CoFe25_9. The process is detailed in 5 steps. Initially, precipitation of hydroxides were made at 100°C as described by Tourinho et al. [45]. We modified this one-step procedure into two steps further described (Step 1 and Step 2).

Step 1 – Hydroxides precipitation. The precipitation of Co(II) and Fe(III) hydroxides is carried out at room temperature. Sodium hydroxyde (4 mmol) solution is added to a mixture of $Co(NO_3)_2{\cdot}6H_2O$ (25 mmol) and $Fe(NO_3)_3{\cdot}6H_2O$ (3 mmol) dissolved in distilled water (80 mL) under stirring. The mixture was kept under vigorous stirring for 30 min and results in nonmagnetic amorphous suspension of hydroxides species.

Step 2 – Ferrite formation. The reaction medium is stirred and heated at 100°C for 2 h. During this step hydroxides transform into cobalt ferrites with sizes ranging between 8 nm and 13 nm [46].

Step 3 – Dispersion in acidic medium. To eliminate spurious non magnetic and amorphous hydroxydes, nitric acid (0.2 mmol, pH = 2) is added to the suspension. This step favor the dispersions of cobalt ferrites, as ($-O^-$) anions initially at the surface after Step 1 are protonated and give ($-OH_2^+$) species. Successive precipitations with acetone were used to remove the excess of acid. As cobalt ferrites are not necessary stable in acidic media, further treatments are used to prevent their degradation[47].

Step 4- Stabilization. Following the Massart process, ferric nitrate is added and the solution is kept boiling during 30 min. The nitrate treatment allows the stable dispersion of cobalt ferrites nanoparticles in acidic medium but leads to the molar ratio $X_M = 25\%$ [48].

Step 5 – Dispersion in aqueous solvent. The ferrites obtained are washed several times with acetone and ether and dispersed in the

Table 1
Physicochemical characteristics of the magnetic iron-cobalt nanospinels. d_0 and σ are the mean diameter and the polydispersity deduced from TEM micrographs,d_{DRX} the particle diameter measured from patterns, X_M the molar ratio and M_S the saturation magnetization measured at 300 K.

Sample	d_0 (nm)	σ	d_{XRD} (nm)	X_M (%)	M_S ($A{\cdot}m^2{\cdot}kg^{-1}$)
CoFe25_7	6.8	0.4	5.4	26.9	65.8
CoFe25_9	8.9	0.5	10.6	26.4	72.8
CoFe33_9	8.6	0.5	10.5	32.7	67.8
CoFe33_11	10.7	0.4	12.8	35.3	72.5
CoFe33_13	13.3	0.4	13.0	35.5	76.2
CoFe33_21	20.9	0.5	18.0	34.2	76.1

aqueous solvent, which yields a colloidal solutions of cobalt ferrites nanoparticles.

Steps 1, 2 and 4 are modified in order to produce, the five other nanospinels than CoFe25_9. A scheme that detailed the steps followed to obtain the six samples is given in Supporting Informations (Fig. S1).

Step 1′. In order to obtain smaller cobalt ferrites nanoparticles, hydroxides precipitation is performed in the presence of complexing species [49]. Step 1 is modified by adding tartrate ions to the mixture of $Co(NO_3)_2{\cdot}6H_2O$ and $Fe(NO_3)_3{\cdot}6H_2O$ before the addition of sodium hydroxide. Step 1′ is used instead of Step 1 to obtain CoFe25_7 ferrofluid.

Step 2′. From the litterature, larger size of nanoparticles can be obtained with hydrothermal treatment [50]. After Step 1, the mixture is transferred into an autoclave reactor set at 200 °C for 1 h. Step 2′ is used instead of Step 2 to obtain CoFe33_13 ferrofluid.

Step 2″. The duration of the hydrothermal treatment influenced the size of the nanoparticles [51]. In Step 2″, the hydrothermal treatment at 200 °C is performed during 24 h in order to obtain larger particles. Step 2″ is used instead of Step 2 to obtain CoFe33_21 ferrofluid.

Step 4′. Chemical composition of $X_M = 33\%$ can be obtain for nanoparticles further dispersed in acidic medium with a cobalt nitrate treatment [52]. Step 4 is modified by adding a solution of Co(II) nitrate (3 mmol) and the mixture is boiled for 30 min. Step 4′ is used in a fraction of the synthesis batch of CoFe25_9 after Step 3 to obtain CoFe33_9.

Step 4″. To obtain a stable ferrofluid at neutral pH, hydroxyl groups at the surface of the particles are exchanged with ligands that ensure long-term stability of ferrofluids combining steric and electrostatic repulsions [49]. Step 4 is modified by adding citrate trisodium salt (3 mmol) to the sol. During citratation the hydroxyl groups at the surface of the particles are replaced by citrate anions. The particles obtained by Step 4″ were dispersed in distilled water in Step 5. Step 4″ is used instead of Step 4 to obtain CoFe25_7, CoFe33_11, CoFe33_13 and CoFe33_21.

2.2. Characterization

2.2.1. Transmission electron microscopy

The morphology of the nanospinels for the six samples has been measured on a JEOL 100 CX2 Transmission Electron Microscope (TEM) (Electronic microscopy platform of the Fédération des Matériaux - UPMC). Fig. 1 shows TEM micrographs and size histograms. The TEM images reveal irregular spheroidal shape nanoparticles for the six samples. The analysis of the diameter of more than 2000 particles for each sample leads to size histograms fitted with a log-normal distribution. Results are reported in Table 1.

2.2.2. X-ray diffraction

The coherent domain size of the nanoparticles were determined with a PANALYTICAL X'pert Pro MPD diffractometer with the CoKα radiation (Kα = 1.79 Å) (See Supporting Information Fig. S2). All diffraction peaks can be indexed with the $CoFe_2O_4$ spinel structure (reference code pattern 96–5941-0064). From the XRD profile of the (311) peak, one can compute the nanospinel size (d_{XRD}) with the Debye-Sherrer expression [53,54]. The mean d_{XRD} sizes are reported in Table 1.

2.2.3. Atomic absorption spectrometry

The cationic concentrations of Cobalt and Iron are determined by Atomic Absorption Spectrometry after degradation of the nanoparticles in concentrated hydrochloric acid. We used a Perkin Elmer Analyst 100 spectrometer with an air-acetylene flame at a mean temperature of 2300°C. Experiments were repeated at least three times on each sample. The molar ratio X_M is determined from the Fe and Co concentrations (Table 1).

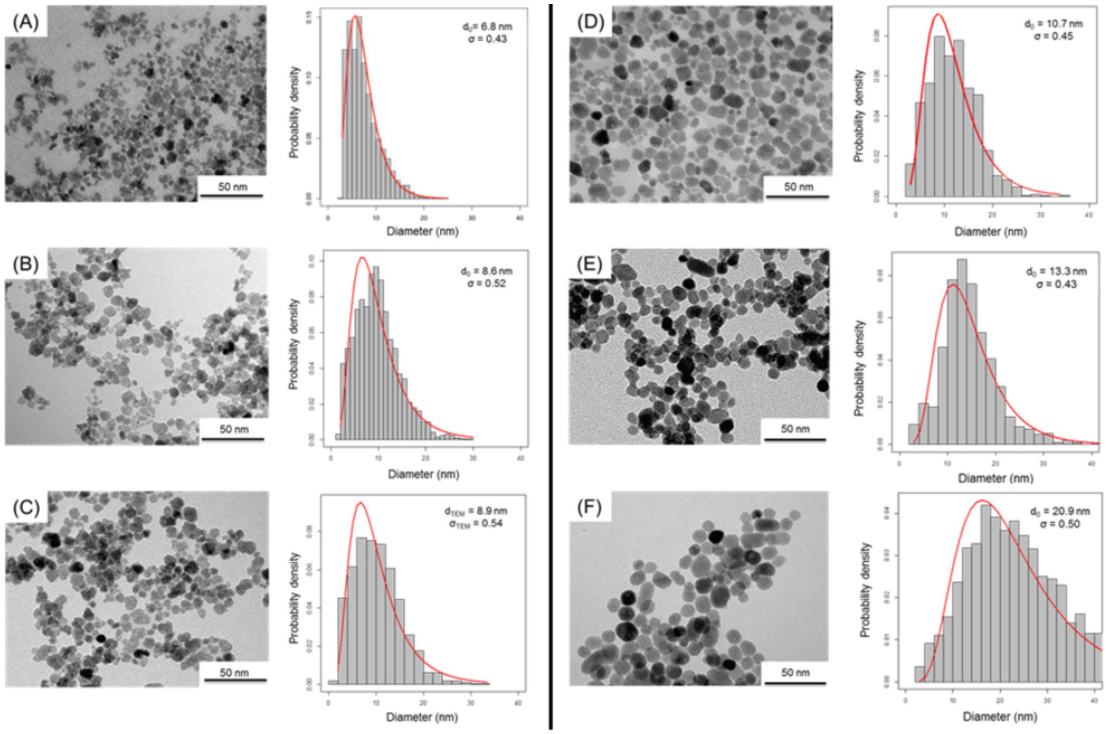

Fig. 1. TEM images and size distribution histograms of (A) 7 nm non-stoichiometric nanoparticles CoFe25_7, (B) 9 nm non-stoichiometric nanoparticles CoFe25_9, (C) 9 nm stoichiometric nanoparticles CoFe33_9, (D) 11 nm stoichiometric nanoparticles CoFe33_11, (E) 13 nm stoichiometric nanoparticles CoFe33_13, (F) 21 nm stoichiometric nanoparticles CoFe33_21.

2.2.4. SQUID magnetometry

Magnetometry measurements were recorded using either a Superconducting QUantum Interference Device (SQUID) Magnetometer (Quantum Design MPMS-XL7) or a Vibrating Sample Magnetometer (QuantumDesign PPMS) (Plate-forme de mesures physiques basse température – UPMC). Measurements are performed on dried powders of nanoparticles at 300 K and 4 K, and on liquid ferrofluids frozen at 4 K. The 4 K magnetization curves for frozen ferrofluids and for dried nanoparticles almost superimpose. The small discrepancies observed between the dried nanoparticles and the ferrofluids measurements show that inter-particles interactions can be neglected in nanoparticles solid phase compare to ferrofluids where colloids are far from each others. Table 1 reports the values of the magnetization at saturation (M_S) for powders nanoparticles at 300 K. Magnetization curves for frozen ferrofluids are plotted in Fig. 4.

2.2.5. X-ray magnetic circular dichroism

XMCD at $L_{2,3}$ edges is a powerful method to probe the *3d* magnetic orbitals of transition metal ions. XMCD possesses the chemical and orbital selectivities of XAS and is sensitive to the site symmetry and the valence of the absorbing atom. XMCD is a magnetic technique that can mostly be explained in the electric dipole approximation so that it chiefly yields information on the orbital magnetic moment of the absorbing atom. When spin–orbit is large enough as it is the case for spin–orbit coupling acting on the 2*p* core–hole, one can also gather information on the spin magnetic moment. As a consequence, it is a unique tool to separate contributions from the different magnetic ions in a ferrimagnetic system such as Iron-Cobalt nanospinels.

XAS and XMCD signals for both Fe and Co $L_{2,3}$ edges were recorded on the DEIMOS beamline at the French synchrotron, SOLEIL [55]. All spectra were measured in Total Electron Yield (TEY) at 4.2 K and in UHV conditions (10^{-10} mbar). In the presence of an external magnetic field H^+ (respectively H^-) parallel (respectively antiparallel) to the X-ray propagation vector, XMCD signals are obtained by taking the difference $\sigma_{XMCD} = \sigma^- - \sigma^+$ where $\sigma^+ = [\sigma_L(H^+) + \sigma_R(H^-)]/2$ and $\sigma^- = [\sigma_L(H^-) + \sigma_R(H^+)]/2$, and σ_L (respectively σ_R) is the absorption cross-section measured with left (respectively right) circularly polarized X-rays. The XMCD signals were recorded by flipping both the circular polarization (either left or right helicity) and the external magnetic field (either +6.6 Tesla or −6.6 Tesla). The circularly polarized X-rays are provided by an Apple-II HU-52 helical undulator for both XAS and XMCD measurements. Ferrofluids are drop-casted on silicon plates and dried at room temperature. The silicon plates are screwed on a non-magnetic sample holder which is entered into the air-lock chamber and transfered into the DEIMOS cryomagnet [55]. Measurements are performed on dried magnetic nanoparticles. For XAS the isotropic absorption cross-section is taken as $\sigma_{Iso} = \frac{\sigma^- + \sigma^+}{2}$. This assumption is fully satisfied for powders of nanoparticles with a cubic crystallographic structure.

By following the variation XMCD intensity as a function of the external magnetic field, one can measure element-specific magnetization curves. One can select energies that correspond to specific spinel sites such as 707.98 eV for Fe ions in T_d sites, 708.72 eV for Fe ions in O_h sites, 776.56 eV for Co ions in T_d sites and 777.55 eV for Co ions in O_h sites. Magnetization curves are measured by using the EMPHU-65 undulator which allows fast switching (5 Hz) of the X-ray circular helicity.

3. Results and discussion

3.1. XAS and XMCD spectra

In Fig. 2 we present the XAS and XMCD spectra of Fe and Co $L_{2,3}$ edges for sample CoFe33_9. The different features of the spectra are labelled to simplify the discussion and the labels are reported in Fig. 2. As expected from the stoichiometry, we notice the absence of Fe^{2+}

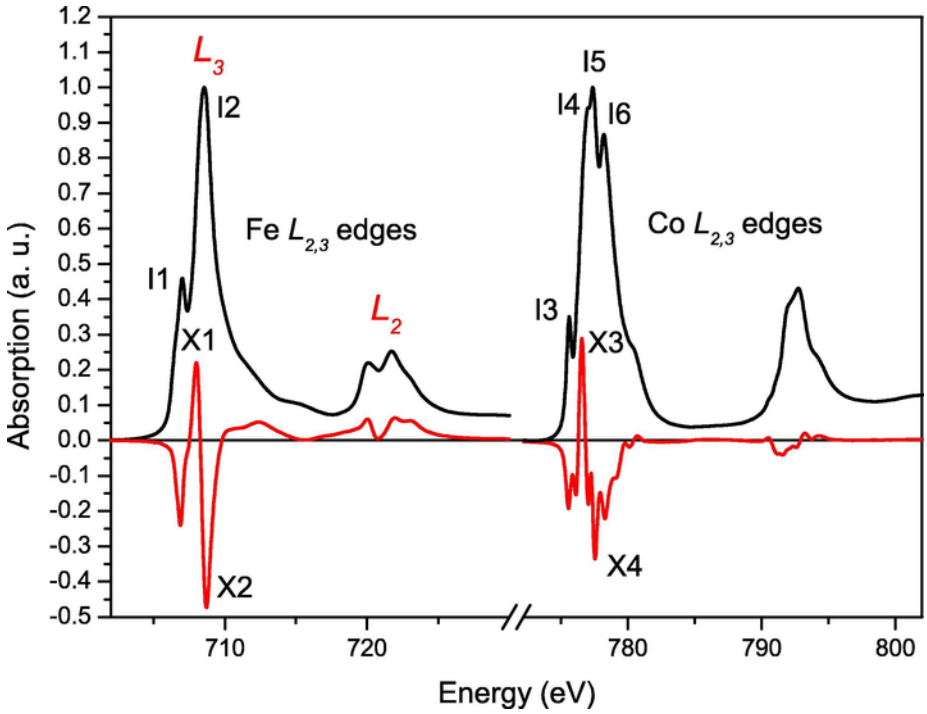

Fig. 2. XAS and XMCD spectra at the Fe (left side) and Co (right side) $L_{2,3}$ edges for the CoFe33_9 sample measured at 4 K with an applied field of ±6.6 Tesla. The different peaks relevant for the discussion have labels beginning with "*I*" for the features of the isotropic spectrum edges and with "*X*" for the features of the XMCD signal.

ions [56]. Iron ions thus exist only as fully oxidized Fe^{3+} ions distributed between T_d and the O_h sites. It is well known from literature that the X1 peak at 707.98 eV is the signature of Fe^{3+} in T_d sites whereas the X2 peak at 708.72 eV is the signature of Fe^{3+} in O_h sites [57]. The corresponding signals have opposite signs which reveal the antiferromagnetic coupling between the T_d sub-lattice and the O_h one. The Co $L_{2,3}$ edges spectra are typical for an iron cobalt spinel containing Co^{2+} ions in both T_d and O_h sites [34]. In the Co^{2+} XMCD spectrum the *X3* peak at 776.56 eV corresponds mainly to the T_d sites (where a small fraction of this positive contribution arises from the signal of the O_h sites – See Fig. S8 in Supporting Informations) while the *X4* peak at 777.54 eV corresponds to the contribution of Co^{2+} in O_h symmetry. All XAS spectra are normalized to 1 at the maximum of the L_3 edge and the XMCD spectra are plotted with respect to the maximum of the isotropic XAS signal. The assignment of the spectral features for Fe and Co $L_{2,3}$ edges is confirmed by Ligand Field Multiplet calculations that have been performed following procedures detailed in previous papers [28,56]. The calculated XAS and XMCD signals can be found in Supporting Informations (Figs. S8 and S9).

Samples are grouped into three sets for the presentation and the discussion of the results. The four samples of the first set (CoFe33_9, CoFe33_11, CoFe33_13 and CoFe33_21) present a stoichiometric composition with a molar ratio $X_M = 33\%$. The second set (CoFe25_7, and CoFe25_9) groups samples with $X_M = 25\%$ where vacancies are present on the O_h sublattice. For the two first sets of samples, the cationic distribution is discussed as a function of size and synthesis route. The third set (CoFe33_9, CoFe25_9) groups the two samples with 9 nm size nanospinels and for which the cationic distribution is examined as a function of two different X_M and two different amounts of vacancies in the O_h sub-lattice.

3.2. *First set – Influence of particle size for $X_M = 33\%$*

The isotropic and XMCD spectra measured at the Fe $L_{2,3}$ edges for samples CoFe33_9, CoFe33_11, CoFe33_13 and CoFe33_21 are plotted in Fig. 3 ((A) and (B) panels). One observes that the ratio *I1/I2* for the isotropic spectra and *X1/X2* for the XMCD signals both increase when the particles size increases. These two variations can be straightforwardly interpreted as an increase of the occupation of the T_d sites with respect to the occupation of the O_h sites when the size of the nanospinels increases. Hence the larger the particles, the higher the fraction of Fe^{3+} on the T_d sites.

The Co spectra measured at the Co $L_{2,3}$ edges can be found in Fig. 3 (panels (B) and (C)). When the size of the nanospinels increase, one observes that peak *I3* and the ratio *I4/I5* increase. As a mirror effect of the *I4/I5* variation, one observes a similar trend at the Co L_2 edge. From Fig. 3, one notices that the intensity of the XMCD feature *X3* increases while *X4* decreases when the size of nanospinels increases. All these variations indicate that the proportion of Co ions in O_h site increases for the larger particle sizes. Hence, the increase of cobalt ions occupancy in O_h sites coincides with the increase of the Fe^{3+} proportion in T_d sites when the size of nanospinels increases.

From SQUID magnetometric measurements reported in Fig. 4, one observes that the larger the nanoparticles, the larger the coercive field. Indeed, the coercive fields are equal to 0.7 Tesla for CoFe33_9 and CoFe33_11 particles, 0.9 Tesla for CoFe33_13 particles and 1.2 Tesla

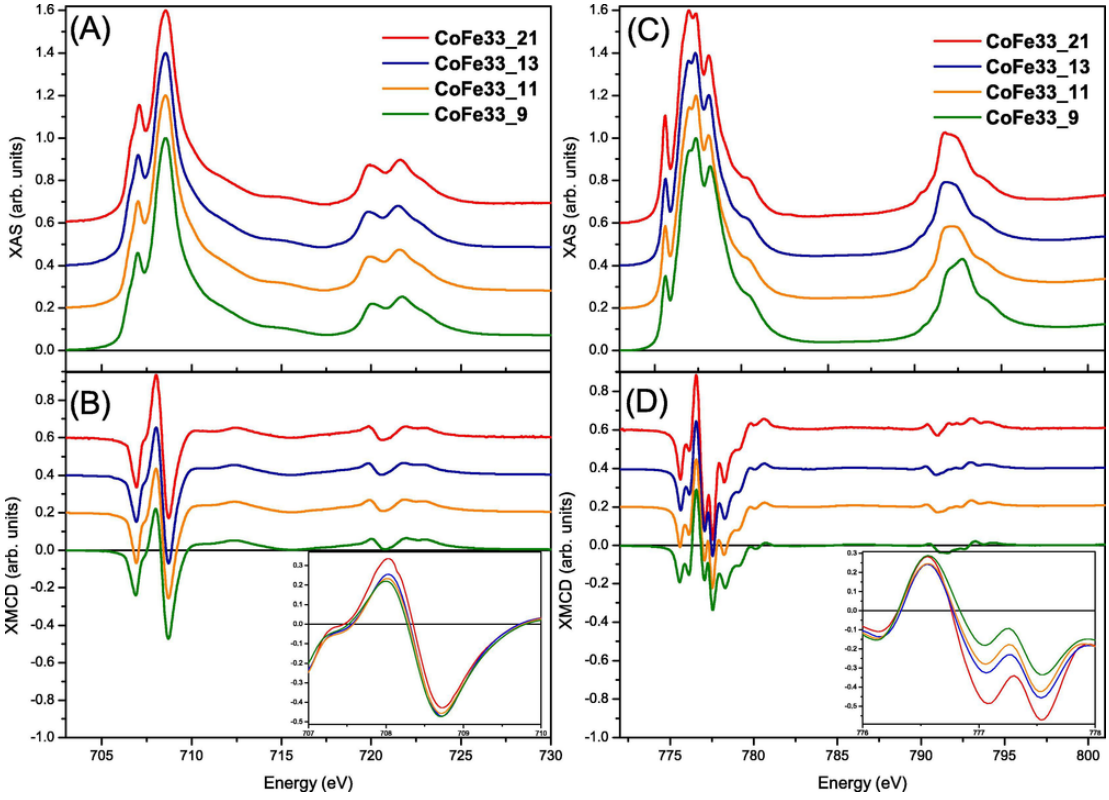

Fig. 3. Isotropic XAS and XMCD spectra at the Fe $L_{2,3}$ edges ((A) and (B)) and Co $L_{2,3}$ edges ((C) and (D)) for CoFe33_9, CoFe33_11, CoFe33_13, CoFe33_21 samples at 4 K. XMCD spectra are plotted in percent of the maximum of the XAS spectra. Inset: zoom in on the L_3 edges of the XMCD spectra.

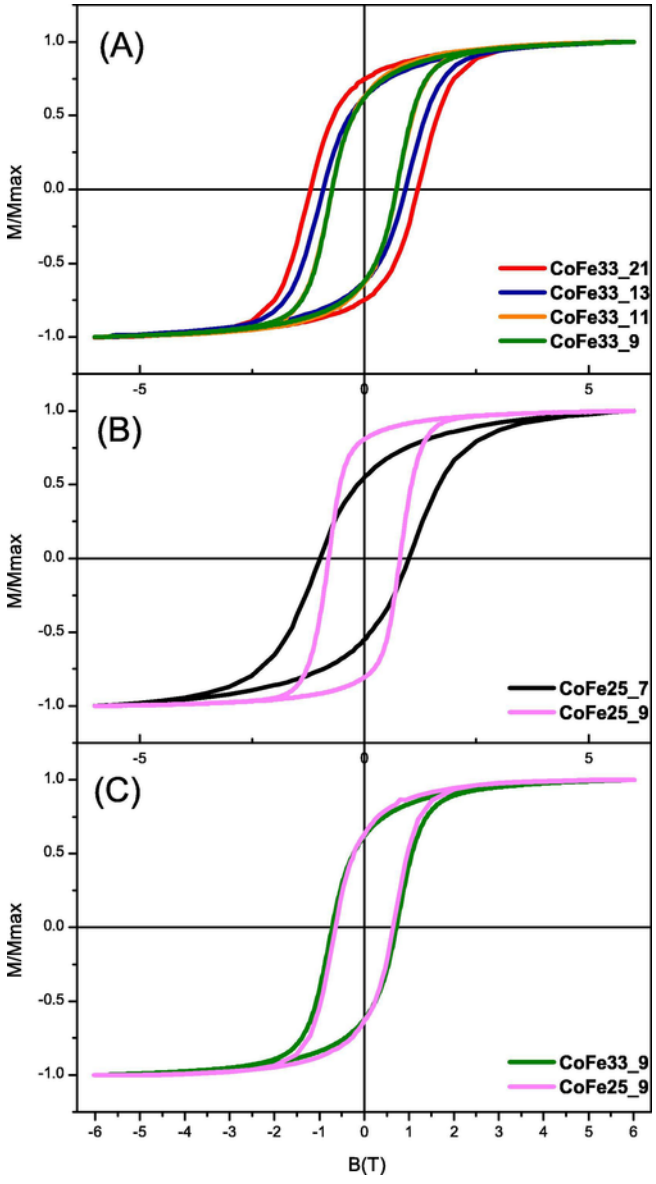

Fig. 4. Magnetization curve versus field measurement of ferrofluids measured at 4K of: CoFe33_9, CoFe33_11, CoFe33_13 and CoFe33_21 (A), CoFe25_9 and CoFe25_7 (B), CoFe25_9 and CoFe33_9 (C).

for CoFe33_21 particles. Same variation is obtained from the XMCD detected magnetization curves (See Supporting Information Fig. S5, see also Table 1). In iron cobalt nanospinels, the magnetic anisotropy mainly arises from the Co ions [58]. For the four different samples with $X_M = 33\%$, the proportion between iron and cobalt ions is constant so that an increase of coercivity cannot be attributed to an increase of Co ions concentration. The Co anisotropy depends on the sites it occupies. The origin of the coercivity for Co ions comes from a strong interplay between spin–orbit coupling and crystal field in O_h symmetry. Indeed the electronic configuration for Co(II) ions is $3d^7$. When the Co(II) ion is in a T_d site, its configuration is $e^4t_2^3$ in the ground state where the e orbitals are at lower energy than the t_2 ones. The corresponding spectroscopic term is $^4A_2$ with no orbital degeneracy thus no orbital moment is expected. On the opposite, when the Co(II) ion is in a O_h site, its configuration is $t_{2g}^5e_g^2$ in the ground state where the t_{2g} orbitals are at lower energy than the e_g ones. The corresponding spectroscopic term is $^4T_1$ which is split by first-order spin–orbit coupling and a large magnetic moment is found in the ground state [59]. Moreover, O_h Co(II) undergoes a strong Jahn–Teller distortion. In the spinel structure, the exact symmetry for the 6-fold site is not O_h but D_{3d} so that Jahn–teller distortion is fully compatible with the crystal structure and the interplay between spin–orbit coupling and crystallographic distortion is then at the origin a large orbital magnetic moment and magnetocrystalline anisotropy for Co ions in distorted O_h symmetry [60]".

Many studies have reported discrepancies of the magnetocrystalline anisotropy observed between the bulk and the nanoparticles in terms of spin-canting [61–63]. Spin-canting arises from the subtle interplay between the chemical disorder, that modifies the superexchange interactions, and the formation of an external layer of non-collinear spin arrangement at the surface of the nanoparticles where the ion coordination symmetry is broken [19,20,64]. In the present case, we have measured magnetization curves by setting the monochromator at energies specific for Fe ions on O_h and T_d sites and for Co ions on O_h and T_d sites. The magnetization curves for one specific sample clearly show the expected antiferromagnetic coupling between O_h and T_d sub-lattices (See Supporting Informations Fig. S4). However, the shape of the curves are exactly the same, so that is no indication for any specific magnetic disorder originating from surface defects. On the other hand, there is a clear indication that the synthesis route that imposes the particle size also induced a different repartition of Co ions between T_d and O_h sites.

From the isotropic and XMCD spectra, we know that when the particle size increases, the amount of Co ions in O_h sites and the amount of Fe ions in T_d sites both increase. Thus in the case of the present series of samples with $X_M = 33\%$, one can conclude that the increase in magnetic anisotropy is governed by larger concentration of Co ions in O_h sites which can be illustrated by a larger inversion parameter γ. Numerical values of γ were calculated from the determination of the cations occupancy in LFM calculations fitted with XMCD experimental data(See the variation of γ in Supporting Informations Table 2). From the co-precipitation synthesis, the variation of γ with the size can be directly related to heat treatments. Heat treatments have already been reported as being at the origin of the cations distribution in $CoFe_2O_4$ [21–23]. Kim et al. have also reported that temperature can increase the coercivity [46]. Here the largest γ is found for the CoFe33_21 which underwent heat treatment at higher temperature of 200°C for several hours. The hydrothermal treatment was already known to increase the size and the crystallinity of the grains. This step also improves the preferential distribution of Co^{2+} ions in O_h sites.

3.3. *Second set – Influence of particle size for $X_M = 25\%$*

CoFe25_7 and CoFe25_9 have been obtained from two rather different synthesis routes leading both to a partial loss of stoichiometry from pure $CoFe_2O_4$ nanospinels. For the two samples CoFe25_9 and CoFe25_7 $X_M = 25\%$ one has [Fe] = 3x[Co]. From the XAS spectra at the Fe $L_{2,3}$ edges one notices that the decrease of divalent cobalt ions is not accompanied by the appearence of divalent iron ions. The presence of vacancies on the O_h sites is therefore expected as it is commonly observed in maghemitizated iron bearing spinels. If the nanospinels are homogeneous with a constant composition (X_M) within the whole particle, then the actual chemical formula is $Fe(III)_{24/11}Co(II)_{8/11}O_4$ which correspond to a small fraction (1/11) of O_h vacancies per formula unit.

In order to account for the degree of inversion, the formula for a sample with $X_M = 25\%$ can be written $\left[\mathrm{Co(II)}_{1-\gamma}\mathrm{Fe(III)}_{\gamma}\right]_{T_d}\left[\mathrm{Co(II)}_{\gamma-3/11}\mathrm{Fe(III)}_{24/11-\gamma}\right]_{O_h}\mathrm{O}_4$. It is to be stressed that if Fe^{2+} ions had been present to compensate the small amount of cobalt, then the stoichiometry formula would have been much different. But in the absence of Fe^{2+}, the chemical composition of cobalt iron nanospinels with $X_M = 25\%$ differs from only 1/11 of vacancies to the ones showing $X_M = 33\%$.

At the Fe $L_{2,3}$ edges, XAS spectra of CoFe25_7 and CoFe25_9 are almost similar with a slight difference in the ratio of *I1/I2* peaks (Fig. 5). XMCD signals for CoFe25_7 and CoFe25_9 particles have also much similar *X3/X4* ratios (Fig. 5) indicating that the distribution of iron ions between the T_d and O_h sites is very similar for both samples. This is slightly different from what has been observed for the samples with $X_M = 33\%$, where a size increase was associated to an increase of Fe ions in the T_d sites. A smaller dichroic amplitude for CoFe25_9 sample compared to CoFe25_7 sample indicates a slightly smaller magnetization. Despite very similar XMCD signals at the Fe $L_{2,3}$ edges, a major difference in the XMCD detected magnetization curve is observed (Fig. 5). The smaller CoFe25_7 particles present a slightly larger coercive field and a much smaller remanent magnetization accompanied by a slanted shape for high fields.

The Co $L_{2,3}$ edges spectra of the CoFe25_7 and CoFe25_9 samples are presented in Fig. 5 panels (C) and (D). At the difference of what has been observed at the Fe $L_{2,3}$ edges, the two spectra present a series of differences that can be readily analyzed as it has been done for the $X_M = 33\%$ series. A sharper *I3* peak, a larger ratio of *I4/I5* and the shape of the L_2 edge (see Fig. S8 in Supporting Informations) indicate that the CoFe25_7 sample contains a larger amount of Co ions in the O_h sites than the CoFe25_9 sample. This trend is fully supported by the XMCD signals at the Co $L_{2,3}$ edges which present a smaller *X3/X4* ratio for CoFe25_7 sample compare to CoFe25_9 sample (see Fig. 5). Contrary to what has been observed for the $X_M = 33\%$ series, one obtains that the larger the particles the smaller the proportion of Co ions on the O_h sites. On the other hand, one sees that the larger the proportion of Co ions in O_h sites, the larger the coercive field and this conclusion is fully satisfied for both $X_M = 33\%$ and $X_M = 25\%$ series (Fig. 4).

3.4. *Influence of the cationic molar ratio* X_M

From the two previous series $X_M = 33\%$ and $X_M = 25\%$, it is clear that the knowledge of the size of the nanoparticles does not give non ambiguous clues concerning the expected magnetic anisotropy or the coercive field. One important physical parameter that scales with the magnetic anisotropy is the content of Co ions in the O_h sites. It then appears interesting to compare the magnetic properties of the two samples with the same size (9 nm) but belonging to the two different series $X_M = 33\%$ and $X_M = 25\%$. Sample CoFe25_9 is obtained from the same synthesis batch as CoFe33_9 except that an excess of Fe(III) nitrate has been added in the case of CoFe25_9 while Co(II) nitrate were used in the synthesis of CoFe33_9 (see Supporting information Fig. S1). Following the analysis developed for the $X_M = 33\%$ series, one notices from the Fe XAS and XMCD signals that the CoFe33_9 sample has a slightly larger proportion of Fe ions in O_h sites (Fig. 3). Similarly, the Co XAS and XMCD signals indicate that the sample with $X_M = 33\%$ has a slightly larger proportion of Co ions in T_d sites (Fig. 6). Interestingly the increase of Co ions in O_h sites does not induce a much larger coercive field for CoFe25_9 compared to CoFe33_9. The shape observed for the Fe and Co isotropic and XMCD signals can be further understood by assuming a core@shell structure for sample CoFe25_9. Iron ni-

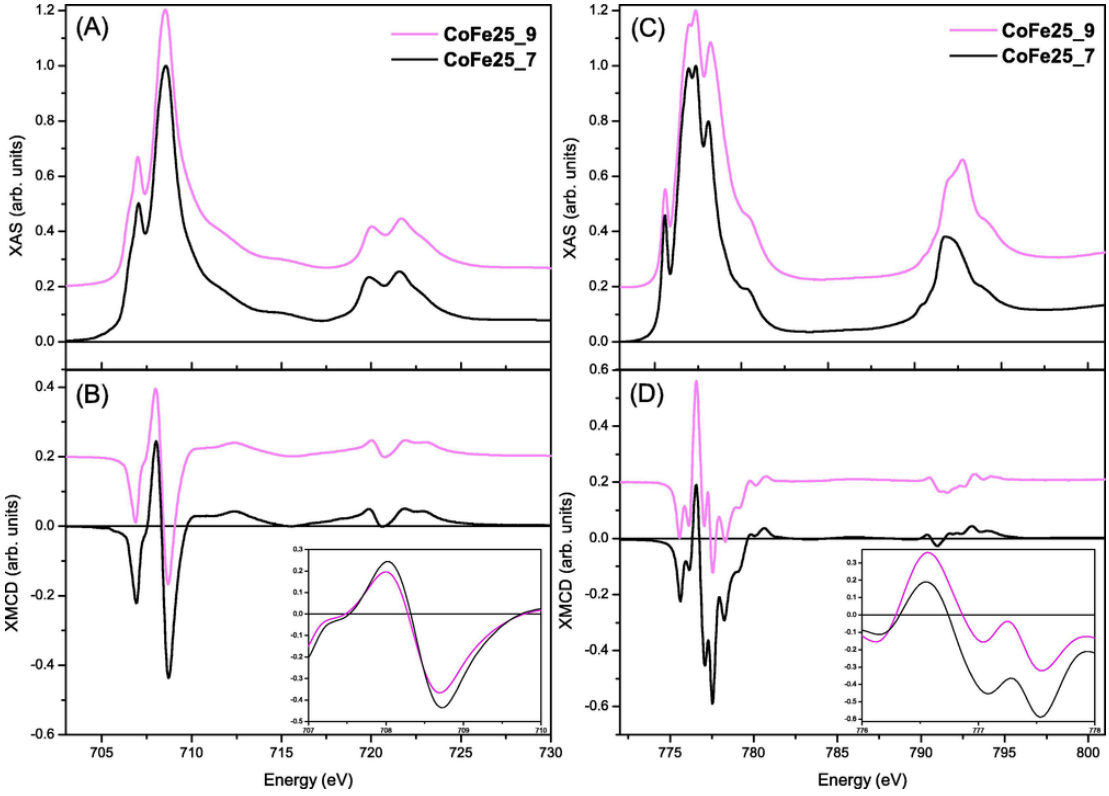

Fig. 5. Isotropic XAS and XMCD spectra at the Fe $L_{2,3}$ edges ((A) and (B)) and Co $L_{2,3}$ edges ((C) and (D)) for CoFe25_7 and CoFe25_9 samples at 4 K.

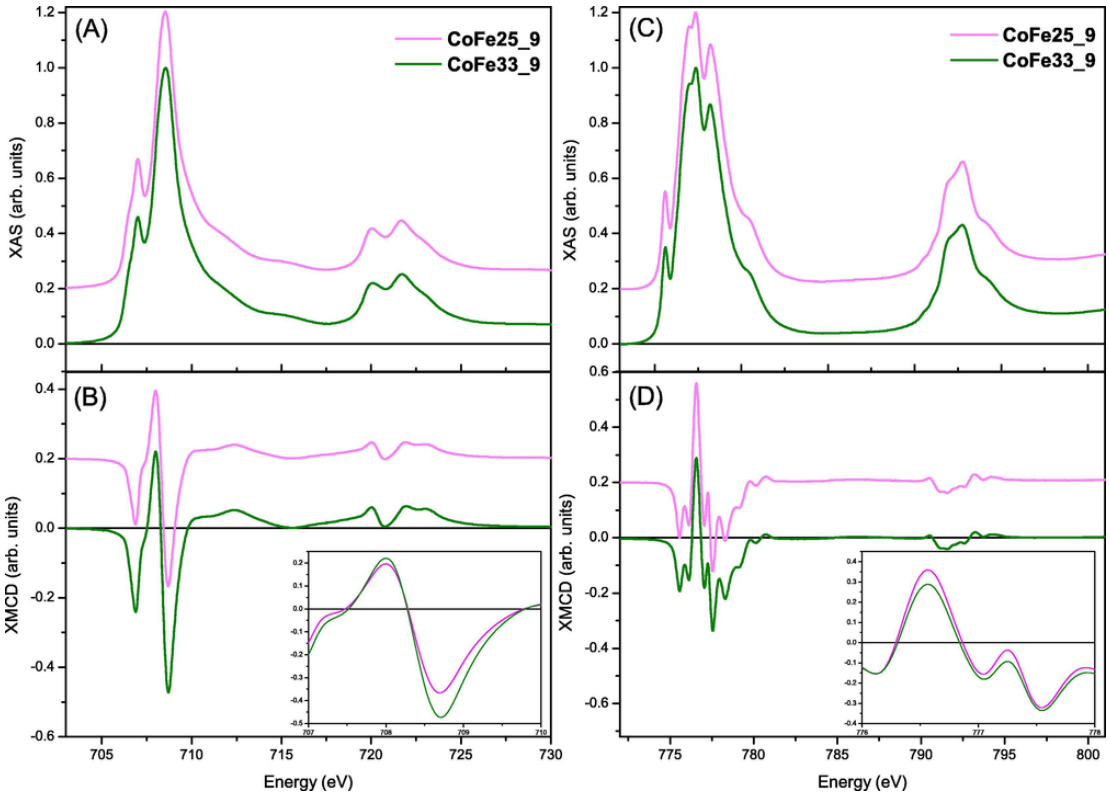

Fig. 6. Isotropic XAS and XMCD spectra at the Fe $L_{2,3}$ edges ((A) and (B)) and Co $L_{2,3}$ edges ((C) and (D)) for CoFe33_9 and CoFe25_9 samples at 4 K.

trates would induce the growth of a small shell of γ-Fe_2O_3 or oxy-hydroxydes in the core of $CoFe_2O_4$ that would contribute to lower the X_M value [52]. The stoichiometry of the core would be then $X_M = 33\%$ with a distribution of the Co ions in O_h sites that is similar to the one observed for CoFe33_9. Another evidence of a core@shell structure for CoFe25_9 nanospinels is brought by calculated sites occupancy performed in the LFM theory (See Table 2 in Supporting Informations). Calculations were performed taking into account the formula $\left[\mathrm{Co(II)}_{1-\gamma}\mathrm{Fe(III)}_{\gamma}\right]_{T_d}\left[\mathrm{Co(II)}_{\gamma-3/11}\mathrm{Fe(III)}_{24/11-\gamma}\right]_{O_h}\mathrm{O}_4$ for CoFe25 samples while cationic distributions in CoFe33 samples are obtained using the formula $\left[\mathrm{Co}_{1-\gamma}\mathrm{Fe}_{\gamma}\right]_{T_d}\left[\mathrm{Co}_{\gamma}\mathrm{Fe}_{2-\gamma}\right]_{O_h}\mathrm{O}_4$. Cationic distributions calculated are consistent with coercive fields measured in XMCD detected magnetic curves (see Supporting Informations Table 2) for all samples except for the CoFe25_9 sample. For the CoFe25_9 nanospinels one obtains a smaller amount of Co^{2+} in O_h sites than for the CoFe33_9 while they show identical coercive fields. One can explain these discrepancies assuming a inhomogeneous chemical composition inside CoFe25_9 nanospinels. In that case, the formula $\left[\mathrm{Co(II)}_{1-\gamma}\mathrm{Fe(III)}_{\gamma}\right]_{T_d}\left[\mathrm{Co(II)}_{\gamma-3/11}\mathrm{Fe(III)}_{24/11-\gamma}\right]_{O_h}\mathrm{O}_4$ cannot be applied for CoFe25_9 as for CoFe25_7 nanospinels which exhibit a steady chemical composition $X_M = 25\%$ in a whole nanospinel.

The comparison of the magnetization curves either measured by SQUID or at the Fe or the Co $L_{2,3}$ edges show that the magnetic properties for the two samples are almost identical. Coercive fields and remanent magnetization are the same with similar general shapes. The main conclusion that can be drawn from the comparison between CoFe33_9 and CoFe25_9 is that when the proportion of Co ions in O_h sites is constant then the magnetization curves are almost identical. This observation further confirms the hypothesis concerning the core@shell structure of sample CoFe25_9. Indeed if the core for CoFe25_9 is similar to CoFe33_9 with a surrounding γ-Fe_2O_3 shell, one would indeed expect that both samples have very similar magnetic properties despite different apparent stoichiometry. On the contrary CoFe25_7 is obtained by blocking the growth of the nanoparticles by adjunction of complexing species agent (tartrate ions). For these very small particles, one would observe a partial, non-congruent dissolution of Co and Fe so that the initial $X_M = 33\%$ stoichiometry is reduced to $X_M = 25\%$. The complexation for this very small particles coupled to a preferential dissolution T_d Co ions would then lead to a larger concentration of Co ions in O_h sites. From a simple geometric estimation, one determines that a surrounding γ-Fe_2O_3 shell of $\approx$0.5 nm accounts for the change of stoichiometry.

4. Conclusion

Magnetic solutions of $CoFe_2O_4$ nanoparticles with different sizes are obtained from the versatile coprecipitation process. Playing with the temperature treatments or with the adjunction of tartrate ions, Fe nitrates or Co nitrates, nanoparticle sizes are tuned between 7 nm and 21 nm. For most syntheses, the expected stoichiometry of 1 Co for 2 Fe ions are obtained, and in two cases the stoichiometry is partially lowered to 1 Co ion for 2 Fe ions. The main outcome of the present study is that neither the size nor the stoichiometry can determine the magnetic properties such as the coercive field nor the remanent magnetization. XMCD allowed the determination of the proportion of Co ions in O_h sites and that this is the parameter governing magnetic coercivity. In addition, the comparison of the data for both Fe and Co $L_{2,3}$ edges showed that some of the particles were very likely built from a core with high Co concentration surrounded by an iron rich shell (probably of γ-Fe_2O_3. Such study could be extend to investigate the intimate relations existing between the magnetic properties and crystallographic structures of magnetic nanoparticles obtain with others synthesis

processes. Inferences to be drawn would helped chemists for the development of rationalized synthesis.

Acknowledgments

This work was supported by French state funds management by the ANR within the Investissements d'Avenir programm under reference ANR-11-IDEX-004–02, and more specifically within the framework of the Cluster of Excellence MATISSE. The authors are very grateful to SOLEIL and the DEIMOS beamline for the good measurement conditions. We express our gratitude to Aude Michel for Atomic Absorption Spectroscopy characterizations and Ludovic Delbes for its technical support on the X-ray Diffractometer.

Appendix A. Supplementary data

Supplementary data associated with this article can be found, in the online version, athttps://doi.org/10.1016/j.jmmm.2018.03.041.

References

[1] I. Torres-Díaz, C. Rinaldi, Recent progress in ferrofluids research: novel applications of magnetically controllable and tunable fluids, Soft Matter. 10 (2014) 8584–8602.

[2] H. Shokrollahi, A. Khorramdin, G. Isapour, Magnetic resonance imaging by using nano-magnetic particles, J. Magn. Magn. Mater. 369 (2014) 176–183.

[3] E.A. Périgo, G. Hemery, O. Sandre, D. Ortega, E. Garaio, F. Plazaola, F.J. Teran, Fundamentals and advances in magnetic hyperthermia, Appl. Phys. Rev. 2 (2015) 041302.

[4] H. Amata, F. Royer, F. Choueikani, D. Jamon, F. Parsy, J.-E. Broquin, S. Neveu, J.J. Rousseau, Hybrid magneto-optical mode converter made with a magnetic nanoparticles-doped SiO_2/ZrO_2 layer coated on an ion-exchanged glass waveguide, Appl. Phys. Lett. 99 (2011) 251108.

[5] Y. Zou, K. Liu, Z. Shen, X. Chen, Magnetic-fluid core optical fiber, Microfluid. Nanofluid. 10 (2011) 447–451.

[6] H.E. Horng, C.S. Chen, K.L. Fang, S.Y. Yang, J.J. Chieh, C.-Y. Hong, H.C. Yang, Tunable optical switch using magnetic fluids, Appl. Phys. Lett. 85 (2004) 5592–5594.

[7] D.S. Mathew, R.-S. Juang, An overview of the structure and magnetism of spinel ferrite nanoparticles and their synthesis in microemulsions, Chem. Eng. J. 129 (2007) 51–65.

[8] N.A. Frey, S. Peng, K. Cheng, S. Sun, Magnetic nanoparticles: synthesis, functionalization, and applications in bioimaging and magnetic energy storage, Chem. Soc. Rev. 38 (2009) 2532.

[9] A.J. Rondinone, A.C.S. Samia, Z.J. Zhang, Characterizing the magnetic anisotropy constant of spinel cobalt ferrite nanoparticles, Appl. Phys. Lett. 76 (2000) 3624–3626.

[10] S. Lefebure, E. Dubois, V. Cabuil, S. Neveu, R. Massart, Monodisperse magnetic nanoparticles: preparation and dispersion in water and oils, J. Mater. Res. 13 (1998) 2975–2981.

[11] D. Caruntu, G. Caruntu, Y. Chen, C.J. O'Connor, G. Goloverda, V.L. Kolesnichenko, Synthesis of variable-sized nanocrystals of Fe_3O_4 with high surface reactivity, Chem. Mater. 16 (2004) 5527–5534.

[12] A. Abou-Hassan, S. Neveu, V. Dupuis, V. Cabuil, Synthesis of cobalt ferrite nanoparticles in continuous-flow microreactors, RSC Adv. 2 (2012) 11263–11266.

[13] T. Hyeon, S.S. Lee, J. Park, Y. Chung, H.B. Na, Synthesis of highly crystalline and monodisperse maghemite nanocrystallites without a size-selection process, J. Am. Chem. Soc. 123 (2001) 12798–12801.

[14] L. Pérez-Mirabet, E. Solano, F. Martínez-Julián, R. Guzmán, J. Arbiol, T. Puig, X. Obradors, A. Pomar, R. Yáñez, J. Ros, et al., One-pot synthesis of stable colloidal solutions of MFe_2O_4 nanoparticles using oleylamine as solvent and stabilizer, Mater. Res. Bull. 48 (2013) 966–972.

[15] R. Massart, Preparation of aqueous magnetic liquids in alkaline and acidic media, IEEE Trans. Magn. 17 (1981) 1247–1248.

[16] Y. Zhang, Z. Yang, D. Yin, Y. Liu, C. Fei, R. Xiong, J. Shi, G. Yan, Composition and magnetic properties of cobalt ferrite nano-particles prepared by the co-precipitation method, J. Magn. Magn. Mater. 322 (2010) 3470–3475.

[17] K. Zhang, T. Holloway, A.K. Pradhan, Magnetic behavior of nanocrystalline $CoFe_2O_4$, J. Magn. Magn. Mater. 323 (2011) 1616–1622.

[18] R.J. Hill, J.R. Craig, G.V. Gibbs, Systematics of the spinel structure type, Phys. Chem. Miner. 4 (1979) 317–339.

[19] D. Peddis, C. Cannas, G. Piccaluga, E. Agostinelli, D. Fiorani, Spin-glass-like freezing and enhanced magnetization in ultra-small $CoFe_2O_4$ nanoparticles, Nanotechnology 21 (2010) 125705.

[20] D. Peddis, N. Yaacoub, M. Ferretti, A. Martinelli, G. Piccaluga, A. Musinu, C. Cannas, G. Navarra, J.M. Greneche, D Fiorani, Cationic distribution and spin canting in $CoFe_2O_4$ nanoparticles, J. Phys.: Condens. Matter 23 (2011) 426004.

[21] G.A. Sawatzky, F.V.D. Woude, A.H. Morrish, Cation Distributions in Octahedral and Tetrahedral Sites of the Ferrimagnetic Spinel $CoFe_2O_4$, J. Appl. Phys. 39 (1968) 1204–1205.

[22] G.A. Sawatzky, F. Van Der Woude, A.H. Morrish, Mössbauer Study of Several Ferrimagnetic Spinels, Phys. Rev. 187 (1969) 747–757.

[23] P.J. Murray, J. Linnett (the late), Mössbauer studies in the spinel system $Co_xFe_{3-x}O_4$, J. Phys. Chem. Solids 37 (1976) 619–624.

[24] D. Peddis, C. Cannas, A. Musinu, A. Ardu, F. Orrù, D. Fiorani, S. Laureti, D. Rinaldi, G. Muscas, G. Concas, et al., Beyond the effect of particle size: influence of $CoFe_2O_4$ nanoparticle arrangements on magnetic properties, Chem. Mater. 25 (2013) 2005–2013.

[25] D. Carta, A. Corrias, A. Falqui, R. Brescia, E. Fantechi, F. Pineider, C. Sangregorio, EDS, HRTEM/STEM, and X-ray absorption spectroscopy studies of co-substituted maghemite nanoparticles, J. Phys. Chem. C 117 (2013) 9496–9506.

[26] M. Artus, L.B. Tahar, F. Herbst, L. Smiri, F. Villain, N. Yaacoub, J.-M. Grenèche, S. Ammar, F. Fiévet, Size-dependent magnetic properties of $CoFe_2O_4$ nanoparticles prepared in polyol, J. Phys.: Condens. Matter. 23 (2011) 506001.

[27] S. Li, V.T. John, C. O'Connor, V. Harris, E. Carpenter, Cobalt-ferrite nanoparticles: structure, cation distributions, and magnetic properties, J. Appl. Phys. 87 (2000) 6223–6225.

[28] J.F. Hochepied, P. Sainctavit, M.P. Pileni, X-ray absorption spectra and X-ray magnetic circular dichroism studies at Fe and Co $L_{2,3}$ edges of mixed cobalt–zinc ferrite nanoparticles: cationic repartition, magnetic structure and hysteresis cycles, J. Magn. Magn. Mater. 231 (2001) 315–322.

[29] N. Kita, N. Shibuichi, S. Sasaki, X-ray magnetic circular dichroism in cobalt–iron spinels and electronic states of Co ions, J. Synchrotron Radiat. 8 (2001) 446–448.

[30] D. Carta, G. Mountjoy, G. Navarra, M.F. Casula, D. Loche, S. Marras, A. Corrias, X-ray absorption investigation of the formation of cobalt ferrite nanoparticles in an aerogel silica matrix, J. Phys. Chem. C 111 (2007) 6308–6317.

[31] C.M.B. Henderson, J.M. Charnock, D.A. Plant, Cation occupancies in Mg Co, Ni, Zn, Al ferrite spinels: a multi-element EXAFS study, J. Phys.: Condens. Matter 19 (2007) 076214.

[32] S. Staniland, W. Williams, N. Telling, G. Van Der Laan, A. Harrison, B. Ward, Controlled cobalt doping of magnetosomes in vivo, Nat. Nanotechnol. 3 (2008) 158–162.

[33] V.S. Coker, C.I. Pearce, R.A. Pattrick, G. van der Laan, N.D. Telling, J.M. Charnock, E. Arenholz, J.R. Lloyd, Probing the site occupancies of Co-, Ni-, and Mn-substituted biogenic magnetite using XAS and XMCD, Am. Mineral. 93 (2008) 1119–1132.

[34] V.S. Coker, N.D. Telling, G. van der Laan, R.A.D. Pattrick, C.I. Pearce, E. Arenholz, F. Tuna, R.E.P. Winpenny, J.R. Lloyd, Harnessing the extracellular bacterial production of nanoscale cobalt ferrite with exploitable magnetic properties, ACS Nano 3 (2009) 1922–1928.

[35] G. Subías, V. Cuartero, J. García, J. Blasco, S. Lafuerza, S. Pascarelli, O. Mathon, C. Strohm, K. Nagai, M. Mito, et al., Investigation of pressure-induced magnetic transitions in Co_xFe_3 - xO_4 spinels, Phys. Rev. B 87 (2013) 094408.

[36] D.K. Kim, J. Dobson, Nanomedicine for targeted drug delivery, J. Mater. Chem. 19 (2009) 6294–6307.

[37] S. Gyergyek, D. Makovec, A. Kodre, I. Arčon, M. Jagodič, M. Drofenik, Influence of synthesis method on structural and magnetic properties of cobalt ferrite nanoparticles, J. Nanopart. Res. 12 (2009) 1263–1273.

[38] G. Aquilanti, A. Cognigni, M. Anis-ur Rehman, Cation distribution in Zn doped cobalt nanoferrites determined by X-ray absorption spectroscopy, J. Supercond. Nov. Magn. 24 (2010) 659–663.

[39] S. Matzen, J.-B. Moussy, R. Mattana, F. Petroff, C. Gatel, B. Warot-Fonrose, J.C. Cezar, A. Barbier, M.-A. Arrio, P. Sainctavit, Restoration of bulk magnetic properties by strain engineering in epitaxial $CoFe_2O_4$ (0 0 1) ultrathin films, Appl. Phys. Lett. 99 (2011) 052514.

[40] J.M. Byrne, V.S. Coker, S. Moise, P.L. Wincott, D.J. Vaughan, F. Tuna, E. Arenholz, G.V.D. Laan, R.A.D. Pattrick, J.R. Lloyd, et al., Controlled cobalt doping in biogenic magnetite nanoparticles, J.R. Soc., Interface 10 (2013) 20130134.

[41] C. Schmitz-Antoniak, D. Schmitz, P. Borisov, F.M.F. de Groot, S. Stienen, A. Warland, B. Krumme, R. Feyerherm, E. Dudzik, W. Kleemann, et al., Electric in-plane polarization in multiferroic CoFe2O4/BaTiO3 nanocomposite tuned by magnetic fields, Nat Commun 4 (2013) 2051.

[42] K.O. Abdulwahab, M.A. Malik, P. O'Brien, G.A. Timco, F. Tuna, C.A. Muryn, R.E.P. Winpenny, R.A.D. Pattrick, V.S. Coker, E. Arenholz, A one-pot synthesis of monodispersed iron cobalt oxide and iron manganese oxide nanoparticles from bimetallic pivalate clusters, Chem. Mater. 26 (2014) 999–1013.

[43] C.I. Pearce, C.M.B. Henderson, R.A. Pattrick, G.V.D. Laan, D.J. Vaughan, Direct determination of cation site occupancies in natural ferrite spinels by L2,3 X-ray absorption spectroscopy and X-ray magnetic circular dichroism, Am. Mineral. 91 (2015) 880–893.

[44] D. Erdem, N.S. Bingham, F.J. Heiligtag, N. Pilet, P. Warnicke, L.J. Heyderman, M. Niederberger, $CoFe_2O_4$ and $CoFe_2O_4$-SiO_2 nanoparticle thin films with perpendicular magnetic anisotropy for magnetic and magneto-optical applications, Adv. Funct. Mater. 26 (2016) 1954–1963.

[45] F.A. Tourinho, R. Franck, R. Massart, Aqueous ferrofluids based on manganese and cobalt ferrites, J. Mater. Sci. 25 (1990) 3249–3254.

[46] Y.I. Kim, D. Kim, C.S. Lee, Synthesis and characterization of $CoFe_2O_4$ magnetic nanoparticles prepared by temperature-controlled coprecipitation method, Phys. B 337 (2003) 42–51.
[47] M.A.G. Soler, E.C.D. Lima, S.W. da Silva, T.F.O. Melo, A.C.M. Pimenta, J.P. Sinnecker, R.B. Azevedo, V.K. Garg, A.C. Oliveira, M.A. Novak, et al., Aging investigation of cobalt ferrite nanoparticles in low ph magnetic fluid, Langmuir 23 (2007) 9611–9617.
[48] F. Tourinho, R. Franck, R. Massart, R. Perzynski, Synthesis and magnetic properties of managanese and cobalt ferrite ferrofluids, Prog. Colloid Polym. Sci. 79 (1989) 128–134.
[49] A. Bee, R. Massart, S. Neveu, Synthesis of very fine maghemite particles, J. Magn. Magn. Mater. 149 (1995) 6–9.
[50] T.J. Daou, G. Pourroy, S. Bégin-Colin, J.M. Grenèche, C. Ulhaq-Bouillet, P. Legaré, P. Bernhardt, C. Leuvrey, G. Rogez, Hydrothermal synthesis of monodisperse magnetite nanoparticles, Chem. Mater. 18 (2006) 4399–4404.
[51] V. Cabuil, V. Dupuis, D. Talbot, S. Neveu, Ionic magnetic fluid based on cobalt ferrite nanoparticles: influence of hydrothermal treatment on the nanoparticle size, J. Magn. Magn. Mater. 323 (2011) 1238–1241.
[52] J.D.A. Gomes, M.H. Sousa, F.A. Tourinho, R. Aquino, G.J. da Silva, J. Depeyrot, E. Dubois, R. Perzynski, Synthesis of core-shell ferrite nanoparticles for ferrofluids: chemical and magnetic analysis, J. Phys. Chem. C 112 (2008) 6220–6227.
[53] P. Scherrer, Bestimmung der Gröe und der inneren Struktur von Kolloidteilchen mittels Röntgenstrahlen, Göttinger Nachrichten Math. Phys. 2 (1918) 98–100.
[54] U. Holzwarth, N. Gibson, The Scherrer equation versus the 'Debye-Scherrer equation', Nat. Nanotechnol. 6 (2011), 534–534.
[55] P. Ohresser, E. Otero, F. Choueikani, K. Chen, S. Stanescu, F. Deschamps, T. Moreno, F. Polack, B. Lagarde, J.-P. Daguerre, et al., DEIMOS: a beamline dedicated to dichroism measurements in the 350–2500 eV energy range, Rev. Sci. Instrum. 85 (2014) 013106.
[56] S. Brice-Profeta, M.A. Arrio, E. Tronc, N. Menguy, I. Letard, C. Cartier dit Moulin, M. Noguès, C. Chanéac, J.P. Jolivet, P. Sainctavit, Magnetic order in – nanoparticles: a XMCD study, J. Magn. Magn. Mater. 288 (2005) 354–365.
[57] C. Carvallo, P. Sainctavit, M.-A. Arrio, N. Menguy, Y. Wang, G. Ona-Nguema, S. Brice-Profeta, Biogenic vs. abiogenic magnetite nanoparticles: a XMCD study, Am. Mineral. 93 (2008) 880–885.
[58] J.C. Slonczewski, Origin of magnetic anisotropy in cobalt-substituted magnetite, Phys. Rev. 110 (1958) 1341–1348.
[59] G. van der Laan, E. Arenholz, R.V. Chopdekar, Y. Suzuki, Influence of crystal field on anisotropic x-ray magnetic linear dichroism at the Co^{2+} $L_{2,3}$ edges, Phys. Rev. B 77 (2008) 064407.
[60] M. Tachiki, Origin of the magnetic anisotropy energy of cobalt ferrite, Prog. Theor. Phys. 23 (1960) 1055–1072.
[61] J.M.D. Coey, Noncollinear spin arrangement in ultrafine ferrimagnetic crystallites, Phys. Rev. Lett. 27 (1971) 1140–1142.
[62] E. Tronc, D. Fiorani, M. Noguès, A.M. Testa, F. Lucari, F. D'Orazio, J.M. Grenèche, W. Wernsdorfer, N. Galvez, C. Chanéac, et al., Surface effects in noninteracting and interacting γ-Fe_2O_3 nanoparticles, J. Magn. Magn. Mater. 262 (2003) 6–14.
[63] C. Vazquez-Vazquez, M.A. Lopez-Quintela, M.C. Bujan-Nunez, J. Rivas, Finite size and surface effects on the magnetic properties of cobalt ferrite nanoparticles, J. Nanopart. Res. 13 (2011) 1663–1676.
[64] D. Peddis, M.V. Mansilla, S. Mrup, C. Cannas, A. Musinu, G. Piccaluga, F. D'Orazio, F. Lucari, D. Fiorani, Spin-canting and magnetic anisotropy in ultrasmall $CoFe_2O_4$ nanoparticles, J. Phys. Chem. B 112 (2008) 8507–8513.